microwave

MDPI

Article

Uniform-Width Slotted mmWave Antenna with Suppressed Sidelobe Level (SLL) and Enhanced Inter-Element Isolation

Jun Zhou, Heng Luo *, Haoran Jia, Yujie Zhang, Huanwei Duan, Huaizhong Chen, Jian Dong, Meng Wang and Chenwang Xiao

School of Electronic Information, Central South University, Changsha 410004, China; 232212088@csu.edu.cn (J.Z.)
* Correspondence: luohengcsu@csu.edu.cn

Abstract

High gain and low sidelobe level remain challenges for 5G millimeter-wave antenna systems. This paper presents a low-sidelobe, high-gain microstrip array antenna based on non-uniformly slotted identical-sized radiating patch, designed to simultaneously enhance gain and suppress sidelobe levels for 5G millimeter-wave (mmWave) communication systems. The key innovation lies in the use of an intermediate-deep, edge-shallow non-uniform slotting technique to precisely control the surface current distribution of the radiating elements, thereby achieving significant sidelobe level (SLL) suppression and antenna isolation enhancement without increasing the physical footprint of each element. The final design operates at a center frequency of 78.5 GHz, achieving a maximum gain of 15 dB and suppressing the first sidelobe below −20 dB, outperforming conventional linear arrays. It is noteworthy that, compared with a Chebyshev-distributed array, the patch width is reduced to only 1 mm, thereby enabling a compact array layout. The unit width dimension is reduced by over 40%, while in a densely packed array configuration, the inter-antenna isolation is increased by more than 18 dB. This current-distribution engineering approach offers a novel, structure-efficient pathway for designing high-performance, densely packed mmWave antenna arrays, circumventing the need for additional decoupling structures or enlarging the antenna spacing. Simulation results show that the average isolation has increased by more than 5 dB from 76 GHz to 79 GHz. Finally, the same design method was used to design a 24 GHz antenna, which was then fabricated and tested. The antenna achieved a sidelobe suppression of −17 dB.

Keywords: millimeter-wave antenna; sidelobe level; slotted patch; high-isolation; surface current distribution

Check for updates

Academic Editor: Changjun Liu

Received: 3 February 2026
Revised: 3 April 2026
Accepted: 7 April 2026
Published: 15 April 2026

Copyright: © 2026 by the authors. Licensee MDPI, Basel, Switzerland. This article is an open access article distributed under the terms and conditions of the Creative Commons Attribution (CC BY) license.

1. Introduction

With the rapid development of intelligent vehicle technology and autonomous driving, automotive mmWave radar, as an important sensor for vehicle distance and speed measurement, is facing increasingly higher performance requirements [1–3]. Automotive mmWave radar mainly operates in the 24 GHz and 77 GHz frequency bands. The 24 GHz radar has a lower cost and mature technology, with a moderate detection range, making it suitable for short- to medium-range applications such as blind spot detection. In contrast, the 77 GHz radar is smaller in size, offers higher accuracy and resolution, and supports longer-range detection, making it more suitable for high-performance requirements such as autonomous driving; however, it comes with higher costs and technical barriers [4,5]. As an important component of radar, the antenna directly affects the radar's detection performance [6].

The higher the antenna gain, the better the radar detection performance, which is also beneficial for improving the signal-to-noise ratio and enhancing radar reliability [7]. Lower SLL can reduce the radar's false alarm rate and improve anti-interference capability [8,9], with Chebyshev array synthesis and Taylor synthesis being common sidelobe suppression methods [10,11].

Faced with complex traffic environments, the gain of a single antenna is relatively small. To enable radar to measure longer distances, array technology holds significant research value [12,13]. Moreover, as radars move toward miniaturized and integrated designs, the antenna layout of the radar RF front end becomes increasingly important. Due to smaller spacing between antennas, strong coupling effects occur between array elements, leading to degraded radiation performance of the antenna system. Some researchers have adopted antenna decoupling structures to enhance isolation between array antennas [14,15].

This paper designs two 1 × 8 mmWave radar array antennas with high gain, high isolation, and low sidelobes, which meet the application requirements for 24 GHz and 77 GHz automotive millimeter-wave radars, respectively. The array antenna uses a series-fed structure, achieving unequal amplitude distribution of current across the antennas by slotting elements of the same width, thereby suppressing sidelobes. Additionally, the antenna layout was analyzed, verifying that this antenna maintains good isolation when integrated into the radar RF front-end layout. Finally, a physical prototype of the 24 GHz antenna array was fabricated and tested, and the test results validated the feasibility of the design scheme.

2. Design of Uniform-Width Slotted Millimeter-Wave Antenna

2.1. Antenna Array Configuration

Figure 1 shows a newly designed uniform-width slotted array antenna operating at 78.5 GHz. As shown in Figure 1a, this antenna consists of three parts: the bottom metal ground plane, the middle dielectric substrate, and the top radiation patch structure, The specific dimensions of the antenna patch are shown in Figure 1b and Table 1 (Table 2 shows the dimensional parameters of the 24 GHz uniform-width slotted antenna). RO3003 was chosen as the dielectric substrate for the uniform-width slotted array antenna. It has an extremely low and stable loss factor of only 0.0013, which minimizes energy loss in the dielectric and ensures that more energy is radiated by the antenna. At the same time, RO3003 has a stable dielectric constant of three. The upper radiation structure mainly consists of eight patch elements connected in series by microstrips, all with the same width. All patch elements except the first one are slotted. The last three antenna elements include an impedance matching structure, and a matching load structure is added at the end of the terminal elements.

The specific antenna design process should first determine the substrate and appropriate thickness according to the operating frequency. The transmission line between the patch and adjacent patches is designed to be half of the effective wavelength. Then, slots are used to change the current distribution to achieve antenna sidelobe suppression. To make the current larger in the middle of the antenna and smaller at both ends, while keeping the radiation pattern as symmetrical as possible and reducing design complexity, the slot depths of the fifth, sixth, and seventh patch elements are the same as those of the fourth, third, and second patch elements (i.e., l_gap3, l_gap2, and l_gap1), but in the opposite direction. Next, an impedance matching structure is designed for the terminal unit. Finally, after completing the design of a single antenna linear array, the antenna layout analysis is carried out.

https://doi.org/10.3390/microwave2020008

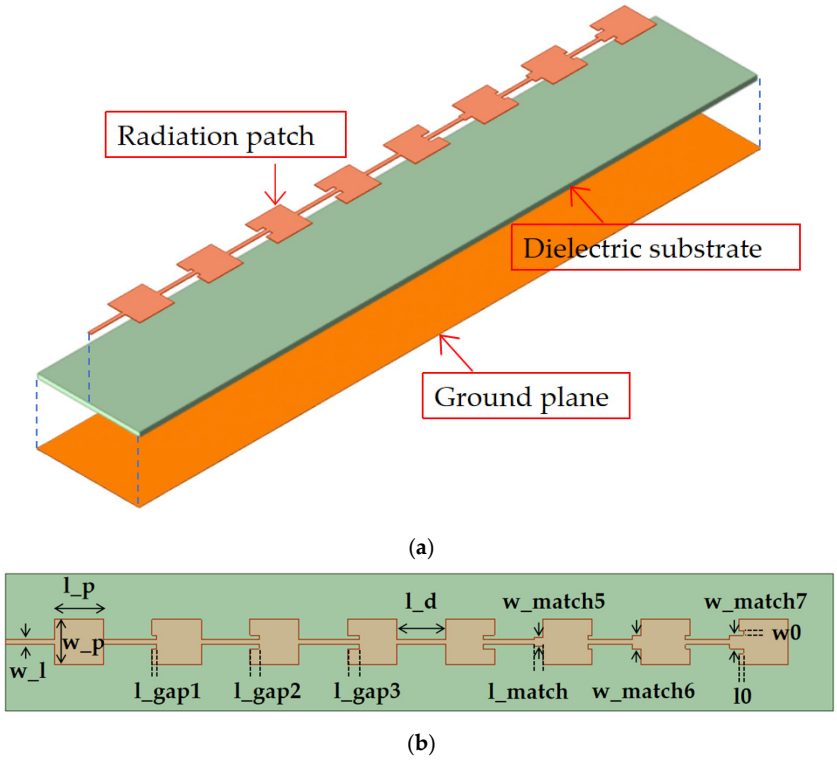


Figure 1. The layout of the 1 × 8 uniform-width slotted microstrip array. (**a**) Antenna oblique three-dimensional structure. (**b**) Antenna top view and dimensional parameters.

Table 1. 78.5 GHz array antenna dimensions. (Units: mm).

Variable	**w_l**	**l_p**	**w_p**	**l_gap1**	**l_gap2**	**l_gap3**	**l_match**
value	0.1	1.08	1	0.1	0.2	0.25	0.2
Variable	**l_d**	**w_match5**	**w_match6**	**w_match7**	**l0**	**w0**	
value	0.97	0.2	0.3	0.3	0.1	0.1	

Table 2. 24.5 GHz array antenna dimensions. (Units: mm).

Variable	**w_l**	**l_p**	**w_p**	**l_gap1**	**l_gap2**	**l_gap3**	**l_match**
value	0.2	3.5	3.6	0.6	0.4	0.6	0.1
Variable	**l_d**	**w_match5**	**w_match6**	**w_match7**	**l0**	**w0**	
value	3.5	0.2	0.2	0.5	0.5	0.3	

2.2. Working Principle of Non-Uniform Slotted mmWave Antenna (78.5 GHz)

In order to achieve high-gain, low-sidelobe performance for microstrip array antennas, the current intensity of different patch elements can be regulated. By reducing the weight of the edge elements, the energy sources that generate harmful coherent interference in non-main lobe directions are effectively weakened, thereby redistributing the radiated energy from the sidelobe regions to the main lobe direction and achieving SLL suppression. According to the principle of microstrip patch antennas, the patch antenna mainly radiates energy from the patch edges, with the current in the transmission line and the patch forming a sinusoidal distribution. To ensure maximum antenna radiation energy, each section of the transmission line and patch is initially designed to be half of the effective wavelength. The current intensity on both sides of the patch unit is equal but opposite in phase, and the current inside the patch unit has a sinusoidal distribution. By setting a

slot at the connection between the patch and the transmission line, the transmission line length connecting the two patches is no longer half of the effective wavelength, and the connection point between the microstrip line and the patch is not at the edge of the patch. At the same time, the introduction of the slot changes the current path on the surface of the patch, causing the current to flow around the edge of the slot, thereby increasing the effective electrical length, lowering the resonance frequency of the patch, and improving the input impedance of the patch. For series-fed arrays, changes in the input impedance of each unit will directly affect the power distributed to each unit by the feed network, thus achieving amplitude weighting.

Figure 2 respectively shows the relationship curves between the antenna SLL and l_gap1, l_gap2, and l_gap3. It is evident that the antenna SLL is significantly influenced by the variation in l_gap1, with smaller l_gap1 resulting in improved sidelobe suppression performance. Regarding the left sidelobe in the antenna radiation pattern, when the l_gap2 is set to 0.1 mm or 0.2 mm, the SLL fluctuation is minimal; however, when the l_gap2 reaches 0.3 mm, the sidelobe suppression effect begins to decrease. In contrast, for the right sidelobe, when the l_gap2 is 0.2 mm, the SLL performance of all lobes is more stable, and the maximum SLL value is also reduced. In contrast, for the side lobe on the right side of the antenna, when the l_gap2 is 0.2 mm, the SLL performance of all lobes is more stable, and the maximum SLL value is also reduced. The relationship between antenna SLL and the variation in l_gap3 follows a pattern analogous to that observed with l_gap2. When the l_gap3 is 0.25 mm, all SLL are relatively even, with a lower maximum SLL. It can be seen that the groove in the middle is slightly deeper, while the groove depth of the patch elements on both sides is slightly shallower, resulting in the best side lobe suppression for the antenna.

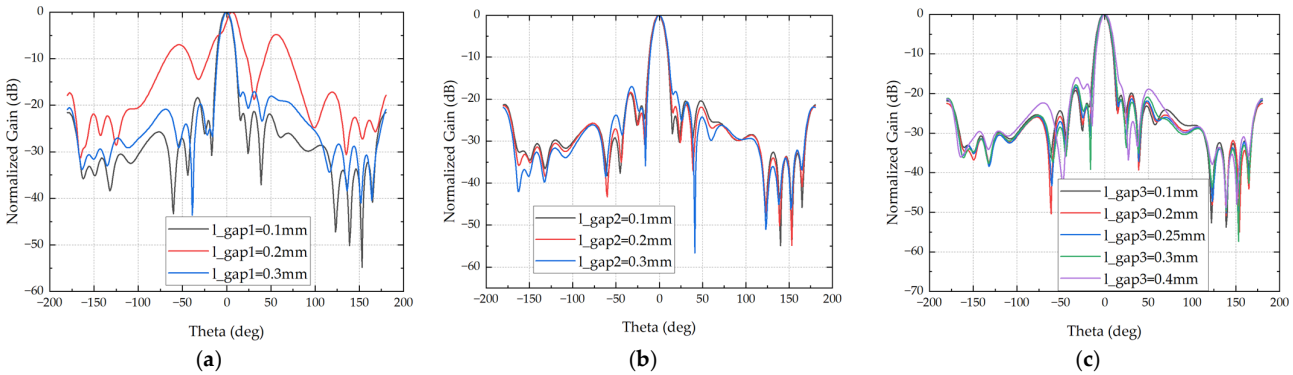


Figure 2. Relationship between antenna SLL and the depth of gap. (**a**) Relationship between antenna SLL and the l_gap1. (**b**) Relationship between antenna SLL and the l_gap2. (**c**) Relationship between antenna SLL and the l_gap3.

To enhance the antenna's impedance matching performance, impedance matching structures are integrated into the last three patch units. This design mitigates the current intensity attenuation in the end patch caused by excessive mutual coupling among array elements. Furthermore, matching load structures are incorporated into the end patch units to absorb residual electromagnetic wave energy, thereby reducing cross-interference with adjacent electronic devices.

Figure 3 respectively shows the antenna S11 parameters and the relationship between SLL and the width of the antenna matching structures. From (a) and (b), it can be observed that when the w_match5 (named according to the fifth patch element) is 0.2 mm, the S11 parameter reaches its minimum, indicating the best matching performance, while the SLL suppression effect is moderate. From (c) and (d), it can be seen that when the w_match6 is 0.3 mm, the S11 parameter reaches its minimum, with little impact on SLL.

When the w_match7 is 0.3 mm, the S11 parameter is also at its minimum, and the SLL suppression effect is at its best. Considering both S parameters and the SLL suppression effect, when the w_match5, w_match6 and w_match7 are 0.2 mm, 0.3 mm, and 0.3 mm, respectively, the antenna loss coefficient is minimized, and the SLL suppression effect is relatively good. It can be observed that having a wider width for the later impedance matching structure units is beneficial for reducing energy loss, allowing a greater portion of the energy to flow smoothly into the end patch element, thereby improving the antenna's radiation performance.

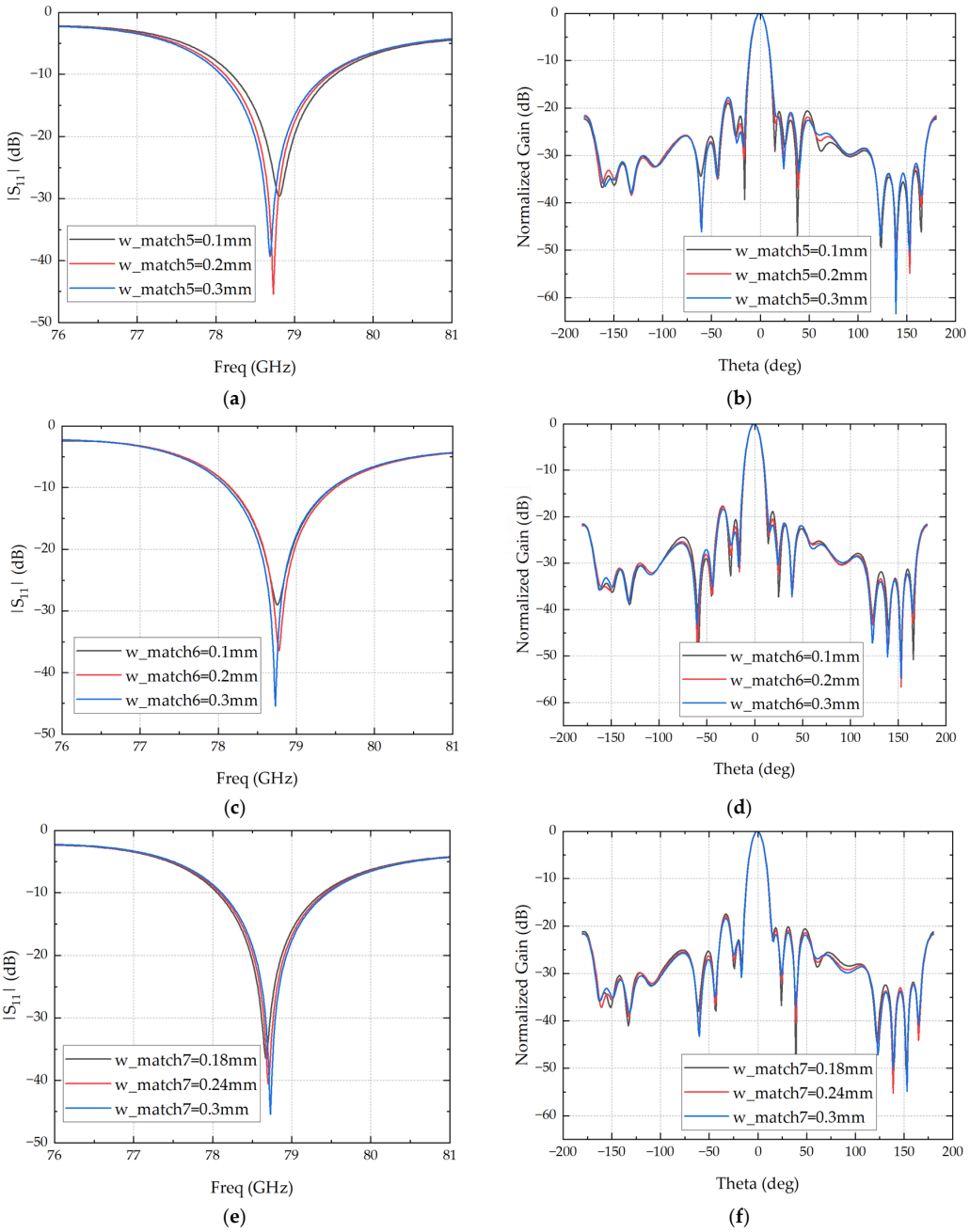


Figure 3. The relationship between antenna S11 parameters and SLL and the width of the antenna impedance matching structure. (**a**) Relationship between antenna S11 parameters and the w_match5. (**b**) Relationship between antenna SLL and the w_match5. (**c**) Relationship between antenna S11 parameters and the w_match6. (**d**) Relationship between antenna SLL and w_match6. (**e**) Relationship between antenna S11 parameters and the w_match7. (**f**) Relationship between antenna SLL and the w_match7.

Figure 4 shows the metal ground surface current density distributions of the uniform-width slotless antenna and the uniform-width slotted antenna. Observation shows that in the absence of slots on the antenna, the current intensity at locations corresponding to individual patches is nearly uniformly distributed. The introduction of slots into the antenna structure enables precise current distribution control, resulting in enhanced current density at the central unit positions while simultaneously suppressing current intensity at the peripheral unit locations. This engineered current modulation effectively concentrates the radiated energy within the main lobe region, thereby achieving significant SLL suppression.

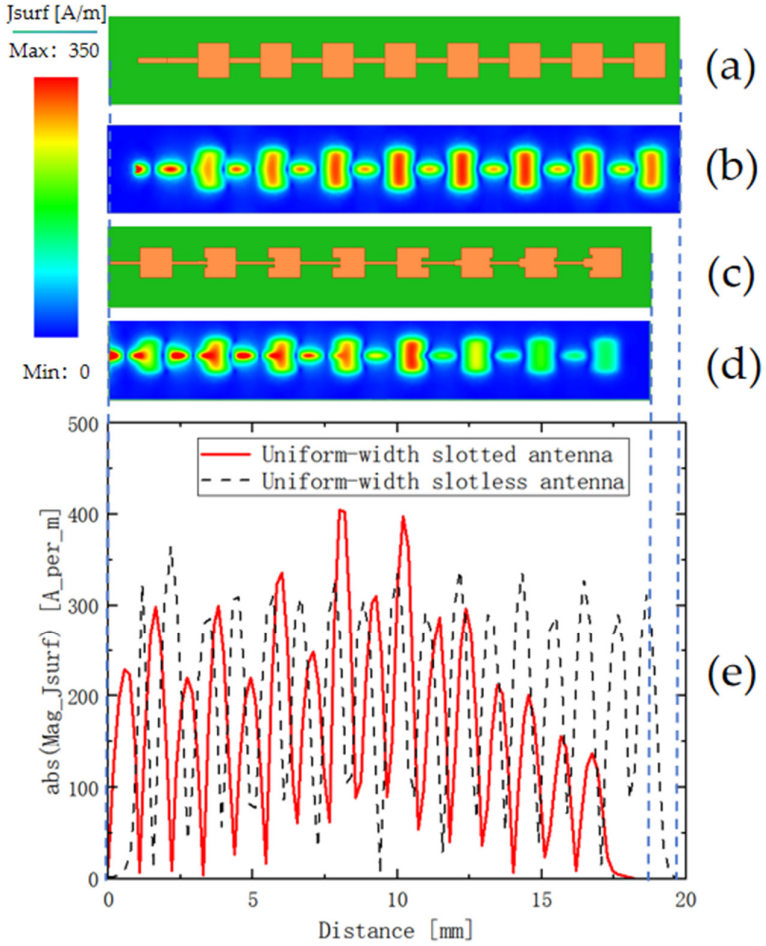
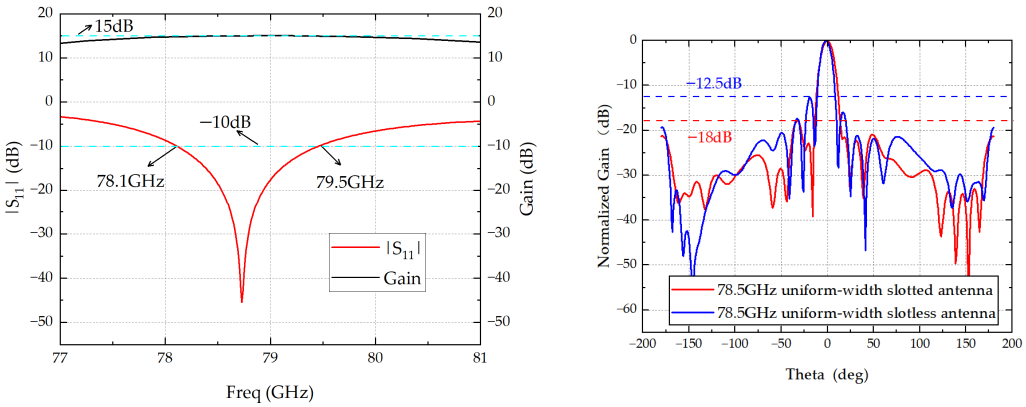


Figure 4. Surface current intensity distribution of antenna metal floor. (**a**) Uniform-width slotless antenna mode. (**b**) Surface current distribution of uniform-width slotless antenna on a metal ground. (**c**) Uniform-width slotted antenna model. (**d**) Surface current distribution of uniform-width slotted antenna on a metal ground. (**e**) Curve of surface current density versus distance from the excitation port for a uniform-width slotted antenna and a uniform-width slotless antenna.

Figure 4a,b correspond to the conventional array antenna model and the metal ground surface current distribution, respectively. It can be seen that the current is relatively evenly distributed across the patches. Figures (c) and (d) correspond to the uniform-width slotted array antenna model and the metal ground surface current distribution, respectively, showing that the current density is higher in the central patch and lower in the patches at both ends. Figure 4e shows the graph illustrating the spatial variation in current intensity along the distance from the feeding port. Each peak in the current distribution profile corresponds to a distinct microstrip line segment and patch unit. The current intensity exhibits a maximum value at the central two patch units and progressively diminishes toward the peripheral regions. Notably, the current density in patch units surpasses that

of the microstrip line due to their wider physical dimensions and consequently lower characteristic impedance, which enables higher current carrying capacity.

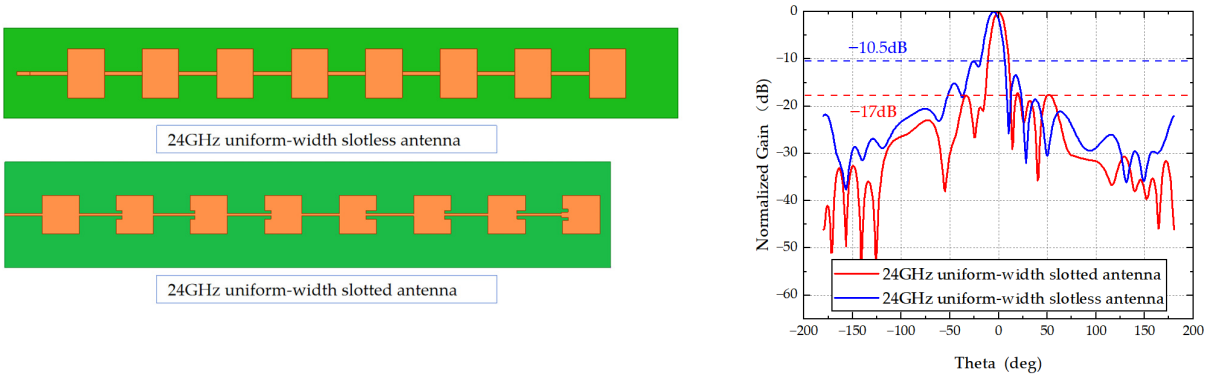
As shown in Figure 5a, the uniform-width microstrip antenna has S11 values below −10 dB in the 78.1 GHz to 79.5 GHz frequency band, indicating good impedance matching. The gain characteristics of the antenna over the frequency range of 76.5 GHz to 81 GHz are also presented, showing that the maximum gain occurs near 78.5 GHz, with a gain value exceeding 15 dB. At the same time, Figure 5b shows that the uniform-width slotted antenna exhibits a clear suppression effect on sidelobe levels compared to conventional antenna. The first sidelobe level is reduced to below −20 dB, and all sidelobe levels are maintained below −18 dB.



(**a**) (**b**)

Figure 5. Performance of uniform-width slotted microstrip array antenna. (**a**) Antenna S11 Parameters and Gain. (**b**) Antenna side lobe level.

Similar to the 78.5 GHz antenna, a uniform-width slotted antenna operating at the 24 GHz frequency was designed using the same method. Figure 6a shows the models of the 24 GHz uniform-width slotless antenna and the uniform-width slotted antenna, respectively, while Figure 6b presents the normalized gain of both antennas. It can be observed that the 24 GHz uniform-width slotted antenna achieves a sidelobe suppression of −17 dB, which is 6.5 dB better than that of the conventional uniform-width slotless antenna, demonstrating that the equal-width slotted structure can effectively reduce the antenna sidelobe levels.

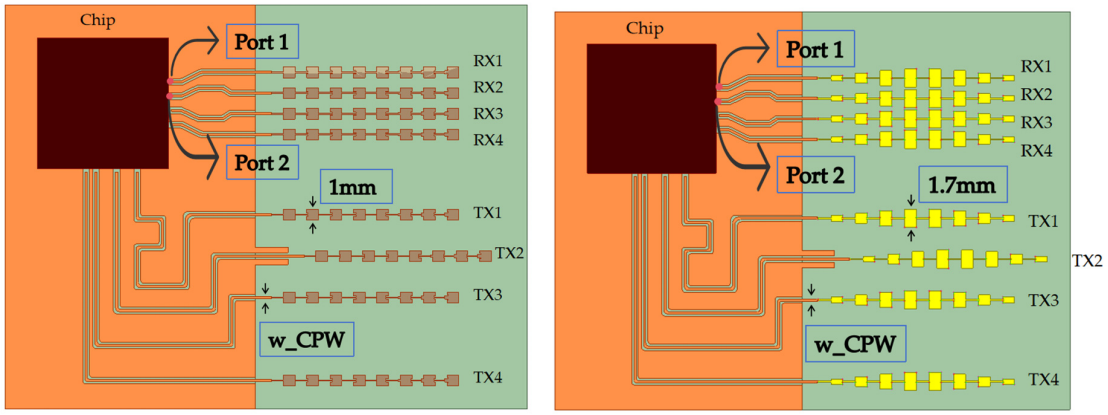


(**a**) (**b**)

Figure 6. 24 GHz uniform-width slotless antenna and 24 GHz uniform-width slotted antenna model and simulation. (**a**) 24 GHz uniform-width slotless antenna and 24 GHz uniform-width slotted antenna mode. (**b**) 24 GHz uniform-width slotless antenna and 24 GHz uniform-width slotted antenna simulation.

3. Analysis of the Layout of Uniform-Width Slotted Microstrip Array Antenna (78.5 GHz)

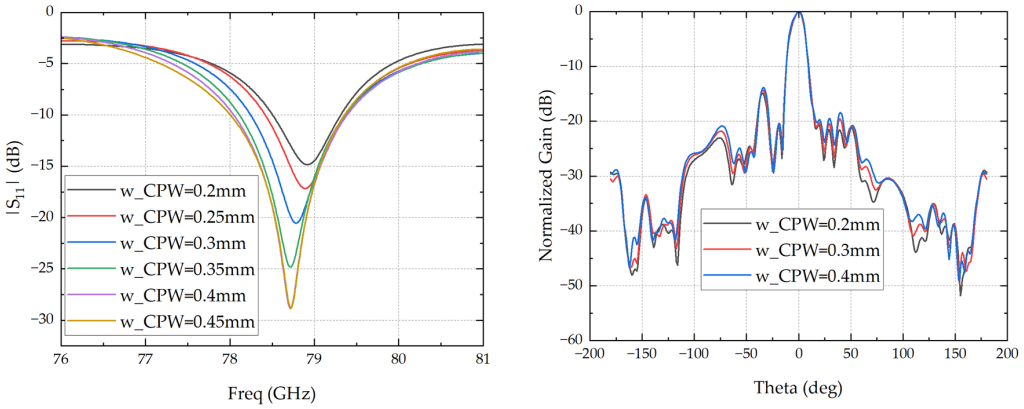
A single-antenna design exhibits inherently limited gain capability and lacks the flexibility to adapt beam patterns to diverse radar detection requirements, thereby failing to satisfy the multi-target detection demands of vehicle-mounted mmWave radar systems. The antenna layout configuration plays a pivotal role in radar performance optimization. As shown in Figure 7, this study conducts layout simulation analysis of both the proposed non-uniform slotted array antenna and the conventional Chebyshev low-sidelobe array antenna based on the antenna architecture of the Texas Instruments AWR2944 mmWave radar chip. The AWR2944 employs a 4 × 4 MIMO (Multiple-Input Multiple-Output) RF front-end configuration, comprising four transmit (TX) and four receive (RX) antenna elements. To ensure phase coherence of signals arriving at each antenna, the transmission lines connecting the chip to the antenna array are meticulously designed with equal electrical lengths. Furthermore, the spatial arrangement of transmit antennas is optimized to achieve two critical objectives: (1) maintaining perfect synchronization between TX and RX antenna pairs, and (2) avoiding both excessive element spacing that leads to area inefficiency and virtual array duplication that degrades spatial resolution. Specifically, the intervals between TX1-TX3 and TX1-TX4 are set to four half-wavelengths (4λ/2), while TX2 is strategically positioned to facilitate elevation angle estimation through phase difference measurement.



(**a**) (**b**)

Figure 7. 4-transmit 4-receive array antenna layout. (**a**) Uniform-width slotted array layout. (**b**) Chebyshev array layout.

To ensure effective signal transmission between the chip and the antenna, a high-performance coplanar waveguide (CPW) is selected as the microstrip transmission line. It consists of a dielectric substrate and three conductors. The middle conductor is a thin metal strip, while the parallel metal strips on both sides, positioned very close to the central conductor, serve as ground conductors. Figure 8a shows the relationship between the width of the intermediate conductor in the CPW (i.e., w_CPW) and the reflection coefficient. As the w_CPW increases, impedance matching improves, but at the same time, the sidelobe suppression of the antenna becomes worse. Therefore, a w_CPW of 0.4 mm is chosen to ensure good impedance matching while maximizing the suppression of the antenna's SLL. Additionally, Figure 8b shows that the SLL on the left side of the antenna are noticeably higher than those on the right side, which is caused by some energy radiating from the CPW on the left side of the antenna.



(**a**) (**b**)

Figure 8. Impact of transmission line width on antenna performance. (**a**) The impact of transmission line width on the antenna reflection coefficient. (**b**) The impact of transmission line width on antenna SLL.

Four receiving antenna arrays are beneficial for improving scalability in multi-array systems, providing a hardware foundation for integrating multiple-input multiple-output (MIMO) or multi-beam applications. In this study, RX1 and RX2 are selected to operate simultaneously in the simulation analysis to evaluate the gain variation in multi-antenna configuration compared with a single antenna, as well as the isolation between antennas. Figure 9 shows the overall antenna gain when RX1 is excited alone versus when both RX1 and RX2 are excited simultaneously. It can be seen that when both ports are excited at the same time, the antenna gain increases, and the antenna beamwidth becomes narrower, resulting in better antenna directivity.

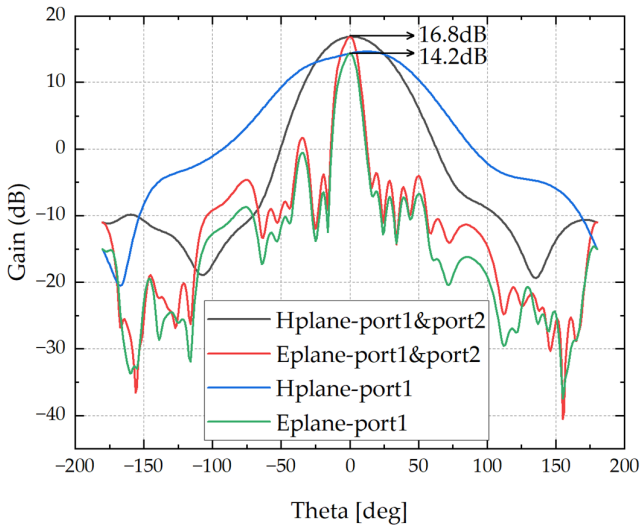


Figure 9. Single-port excitation and dual-port excitation antenna gain.

Figure 10 shows the curves of the S21 parameters of the two antennas versus frequency. It can be seen that the slotted low-sidelobe array antenna designed in this paper has an S21 parameter that is on average more than 5 dB lower in the 76–79 GHz range compared to the traditional Chebyshev low-sidelobe array antenna, and the isolation between antennas is better. This is because the maximum unit size of the array patch designed in this paper is only 1 mm (As shown in Figure 7a), which is approximately 40% smaller than the maximum width of 1.7 mm of the Chebyshev array patch (As shown in Figure 7b). With the spacing between the two antennas kept equal, the patches in the Chebyshev array are closer together, resulting in stronger coupling effects between adjacent antennas.

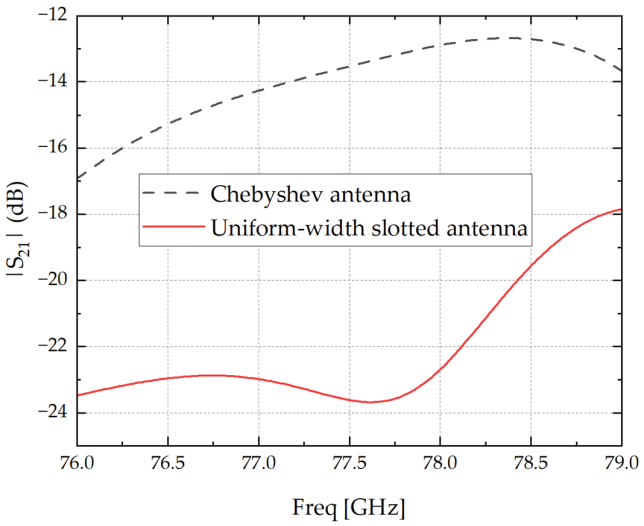
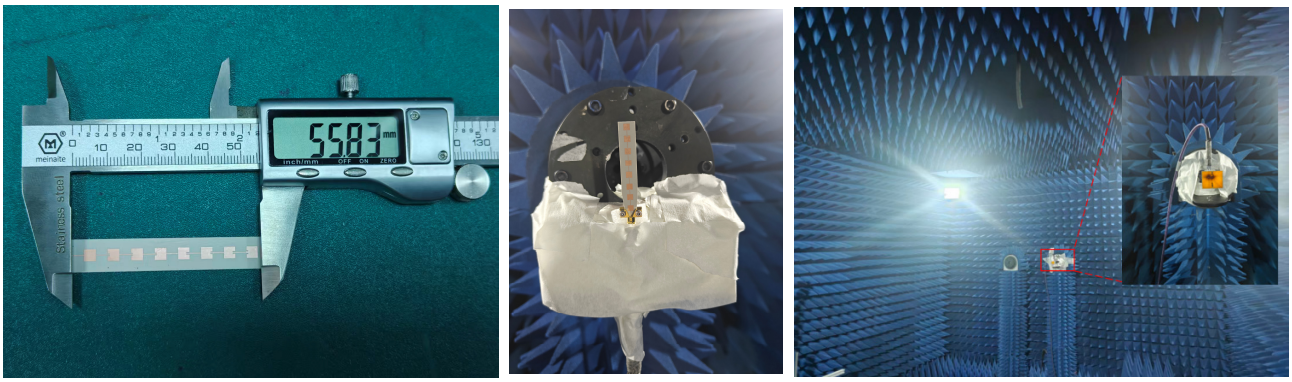


Figure 10. Comparison of isolation between uniform-width slotted antenna and Chebyshev array antenna.

4. Implementation and Measurement

Due to the high cost of manufacturing 77 GHz array antennas and the stringent requirements of the testing equipment, in order to verify the feasibility of the above design scheme, we conducted a fabrication test on a 24 GHz array antenna. The finished antenna array is shown in Figure 11a. The antenna is composed of upper and lower copper foils and a middle RO3003 dielectric substrate, and its surface is treated for oxidation resistance. It is connected to the antenna feed line with a solderless adapter for easy testing. After calibrating the vector network analyzer, it is connected to the antenna via a coaxial cable, allowing accurate measurement of the antenna's return loss. As shown in Figure 11b,c, in this study, a point-to-point method is used to test the antenna's radiation pattern. The testing system consists of an anechoic chamber, a vector network analyzer, a turntable, and other components, providing accurate test results. During antenna testing, the antenna is connected to the vector network analyzer via a coaxial cable, and the turntable is controlled to rotate the antenna, obtaining the antenna radiation pattern on different azimuth planes. By comparing the measured radiation pattern of the antenna under test with the radiation pattern received by a standard horn antenna, the actual radiation pattern of the antenna under test can be determined.



(**a**) (**b**) (**c**)

Figure 11. Antenna physical object and testing. (**a**) Antenna physical object. (**b**) Tested antenna. (**c**) Anechoic chamber test environment, standard speaker antenna used for testing the antenna under test.

Figure 12 shows the simulation and test results of a uniform-width slotted antenna. It can be seen that this antenna mainly operates in the 24 GHz frequency band, with a return loss coefficient below −15 dB at 24 GHz. By adopting a uniform-width non-uniform slotted structure design, the measured gain of this antenna reaches 12.5 dB, while also demonstrating excellent sidelobe suppression performance, with the overall sidelobe suppression level below −17 dB. The simulation and test results show a high degree of correlation, but there are some fluctuations. This is because millimeter-wave antennas are small in size and may have certain dimensional errors during fabrication, and the antenna is relatively thin, making it prone to bending and other unstable factors that cause errors.

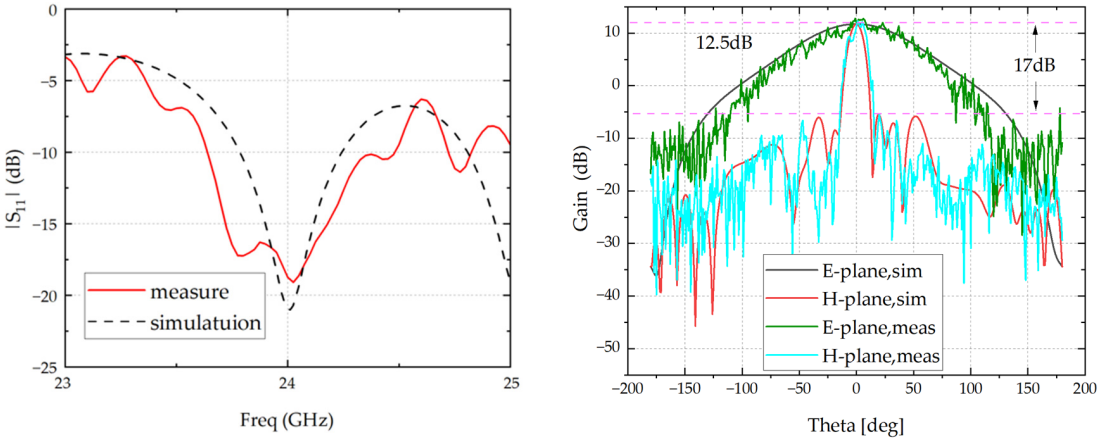


Figure 12. Antenna physical model and test results. (**a**) |S11|. (**b**) Normalized gain.

5. Conclusions

This paper proposes a novel design method for high-gain, low-sidelobe microstrip uniform-width array antennas. The antenna adopts a non-uniform slot structure, with deep slots in the middle patch elements and shallow slots in the side elements, effectively regulating the antenna current distribution, thereby better focusing energy on the main beam and achieving efficient suppression of sidelobe levels. Additionally, for the last three patch elements, an impedance matching structure is designed to better direct energy into the terminal patch element. Based on this method, an antenna was designed that achieves good impedance matching in the 78.1 GHz to 79.5 GHz frequency band, with a gain of 15 dB and overall sidelobe levels suppressed below −18 dB. This paper also conducts a layout analysis of the designed antenna. Compared with a single antenna, reasonably increasing the number of antennas and adopting a proper layout method can further enhance antenna gain. Due to the unique uniform-width structure of the antenna patches, compared with traditional Chebyshev low-sidelobe array antennas, the maximum width is smaller, allowing for larger spacing between antennas and improving inter-antenna isolation. Simulation results show that the uniform-width array antenna with added slots achieves an average improvement of about 5 dB in isolation compared with the Chebyshev array antenna from 76 GHz to 79 GHz. As shown in Table 3, compared with other literature, the antenna designed in this paper has both high gain and low sidelobe characteristics, and the antenna layout is considered, which is conducive to the integration of the radar front end.

Finally, an array antenna operating at 24 GHz was fabricated using the same equal-width grooved design method. The antenna's sidelobe levels were suppressed below −17 dB, verifying the effectiveness of the antenna design method.

Table 3. Comparison between this work and previous publications.

Ref.	Frequency (GHz)	Gain (dB)	SLL (dB)	Array Layout Analysis
[2]	78.5	15.5	−15.5	yes
[16]	77.7	6.43	no	no
[17]	26	8.42	no	yes
[18]	20/26/39	12.5	no	no
[19]	31	9.8	no	yes
[20]	28	13.8	no	no
[21]	39	10	no	no
This work	78.5	15	−18	yes
This work	24	12.5	−17	no

Author Contributions: Simulation optimization, validation, formal analysis, writing—original draft, and visualization were performed by J.Z. Resource coordination, writing—review and editing, supervision, and funding acquisition were carried out by H.L. Problem-solving assistance was provided by H.J., Y.Z., H.C., H.D., J.D., M.W. and C.X. All authors have read and agreed to the published version of the manuscript.

Funding: This work was funded in part by the National Natural Science Foundation of China under Grant 61801521 and Grant 61971450, and in part by the Natural Science Foundation of Hunan Province under Grant 2018JJ2533, Grant 2022JJ30052, and Grant 2023JJ40775.

Data Availability Statement: The raw data supporting the conclusions of this article will be made available by the authors on request.

Acknowledgments: In the course of this research, the authors utilized software tools including Ansys HFSS (version 2026 R1) for electromagnetic modeling and optimization analysis, and Origin 2026 SR1 (version 10.3.0.197) for data visualization and graphical presentation of results. The capabilities of these software packages were instrumental in facilitating the study and effectively communicating the findings, for which the authors express their gratitude.

Conflicts of Interest: The authors declare no conflicts of interest.

Abbreviations

The following abbreviations are used in this manuscript:

SLL	suppressed sidelobe level
mmWave	millimeter-wave
CPW	coplanar waveguide

References

1. Cai, Y.; Bai, J.; Shen, H.L.; Huang, L.; Rao, B.; Wang, H. Development of Low-Cost Single-Chip Automotive 4D Millimeter-Wave Radar. *Sensors* **2025**, *25*, 4640. [CrossRef] [PubMed]
2. Sakurai, R.; Hirokawa, J.; Tomura, T. Waveguide 3 × 2-slot subarray antenna for millimeter-wave car radar. *IEICE Commun. Express* **2025**, *14*, 155–158. [CrossRef]
3. Tan, B.; Ma, Z.; Zhu, X.; Li, S.; Zheng, L.; Huang, L.; Bai, J. Tracking of Multiple Static and Dynamic Targets for 4D Automotive Millimeter-Wave Radar Point Cloud in Urban Environments. *Remote Sens.* **2023**, *15*, 2923. [CrossRef]
4. Bu, D.; Qu, S.-W. Magneto-electric dipole antenna array for 77 GHz automotive radar. *IET Microw. Antennas Propag.* **2023**, *18*, 96–105. [CrossRef]
5. Chen, Q.; Yan, S.; Guo, X.; Wang, W.; Huang, Z.; Yang, L.; Li, Y.; Liang, X. A low sidelobe 77 GHz centre-fed microstrip patch array antenna. *IET Microw. Antennas Propag.* **2023**, *17*, 887–896. [CrossRef]
6. Zhang, Y.; Zhang, J. Design of a Novel Ultra-Wideband Antipodal Vivaldi Antenna Based on Klopfenstein Curve. *Microwave* **2025**, *1*, 4. [CrossRef]
7. Yong, S.A.; Boumseock, K. High Gain Diagonally-Probe-Fed Multi-Layered Dielectric Resonator Antenna Array for 77 GHz Automotive Radar Applications. *J. Infrared Millim. Terahertz Waves* **2024**, *45*, 349–369. [CrossRef]

8. Zhou, J.; Wang, Q.; Yang, Y.; Li, Y.; Kang, K.; Tang, H. A 77 GHz Millimeter-Wave Comb Antenna With Suppressed Side-Lobe. *Microw. Opt. Technol. Lett.* **2025**, *67*, e70185. [CrossRef]
9. Zhu, J.; Liu, J. Design of Microstrip Antenna Integrating 24 GHz and 77 GHz Compact High-Gain Arrays. *Sensors* **2025**, *25*, 481. [CrossRef]
10. Li, L.; Dong, Y.; Cai, X.; Tian, J. An Antenna Array with Wide Flat-Top Beam and Low Sidelobes for Aerial Target Detection. *Sensors* **2025**, *25*, 5991. [CrossRef]
11. Jung, J.; Park, Y.; Ryu, J. Enhanced Phase Coherence in Series-Fed Patch Array Antenna: A Design Method for Uniform Element Spacing With Low Sidelobe Levels. *Microw. Opt. Technol. Lett.* **2024**, *66*, e70066. [CrossRef]
12. Rajpoot, S.; Baghel, S.G.; Swati, M. Design of a compact, wideband, Diagonal Square Fractal MIMO antenna for vehicular communication. *AEU-Int. J. Electron. Commun.* **2025**, *202*, 156023. [CrossRef]
13. Pillai, J.; Prajapati, J.; Upadhayay, D.M. Wide Half Power Beamwidth MIMO Antenna for Vehicular Radar System. *Int. J. Appl. Electromagn. Mech.* **2025**, *77*, 276–290. [CrossRef]
14. Kuriyama, A.; Nagaishi, H.; Kuroda, H.; Kitayama, A. Horn and Lens Antenna with Low Height and Low Antenna Coupling for Compact Automotive 77-GHz Long-Range Radar: Special Section on Microwave and Millimeter-Wave Technologies. *IEICE Trans. Electron.* **2020**, *E103.C*, 426–433. [CrossRef]
15. Bakhshi, M.; Faramarzi, V.; Ayatollahi, H.S.; Mollaee, M. Enhanced 2-port MIMO antenna with composite two-step metasurface for 77 GHz Vehicle-to-Everything applications. *AEU-Int. J. Electron. Commun.* **2024**, *184*, 155404. [CrossRef]
16. Chaudhary, S.; Kansal, A. ADAS radar antenna for mmW/THz communication. *Analog Integr. Circuits Signal Process.* **2025**, *124*, 37. [CrossRef]
17. Khan, M.I.; Khan, M.K.; Rahman, S.U.; Anab, M.; Basit, A. Quad Ports Millimeter-Wave MIMO Antenna With Parasitic Element and Defected Ground Structure for Radar Sensing Application. *Radio Sci.* **2025**, *60*, e2024RS008174. [CrossRef]
18. Chen, Q.; Cheng, F.Y.; Liao, C.; Zhong, X. Triple-band shared-aperture antenna integrating Fabry–Pérot radiator and microstrip grid array for millimeter-wave communication applications. *AEU-Int. J. Electron. Commun.* **2025**, *200*, 155866. [CrossRef]
19. Mani, S.; Paik, H. A six-port High Isolation millimeter wave MIMO antenna based on Array-antenna Decoupling Surface for Next-Generation Wireless Networks. *AEU-Int. J. Electron. Commun.* **2025**, *196*, 155810. [CrossRef]
20. Khouyaoui, I.; Elbathaoui, M.; Hamdaoui, M.; Foshi, J. Design, simulation, and fabrication of high-gain microstrip patch antenna arrays for 28 GHz millimeter-wave 5G applications. *Phys. Scr.* **2025**, *100*, 045218. [CrossRef]
21. Nasri, H.E.N.; Das, S.; Ghzaoui, E.M.; Algarni, A.D.; Madhav, B.T.P.; Fattah, M. A Metamaterial (MTM) Array Antenna Featuring High Gain and Super Wide Bandwidth for mm-Wave 5G NR n257/n260/n261 Networks Applications. *J. Electron. Mater.* **2024**, *54*, 3111–3129. [CrossRef]

Disclaimer/Publisher's Note: The statements, opinions and data contained in all publications are solely those of the individual author(s) and contributor(s) and not of MDPI and/or the editor(s). MDPI and/or the editor(s) disclaim responsibility for any injury to people or property resulting from any ideas, methods, instructions or products referred to in the content.